Synthetic and Systems Biotechnology 8 (2023) 741–748

Contents lists available at ScienceDirect

Synthetic and Systems Biotechnology

journal homepage: www.keaipublishing.com/en/journals/synthetic-and-systems-biotechnology

Original Research Article

Efficient stereoselective hydroxylation of deoxycholic acid by the robust whole-cell cytochrome P450 CYP107D1 biocatalyst

Chixiang Sun [a,b,c,d], Baodong Hu [a,b,c,d], Yanchun Li [b,e], Zhimeng Wu [b,e], Jingwen Zhou [a,b,c,d], Jianghua Li [a,b,c,d], Jian Chen [a,b,c,d], Guocheng Du [a,b,c,d,e,**], Xinrui Zhao [a,b,c,d,*]

[a] Science Center for Future Foods, Jiangnan University, 1800 Lihu Road, Wuxi, Jiangsu, 214122, China
[b] Key Laboratory of Industrial Biotechnology, Ministry of Education, School of Biotechnology, Jiangnan University, 1800 Lihu Road, Wuxi, Jiangsu, 214122, China
[c] Jiangsu Province Engineering Research Center of Food Synthetic Biotechnology, Jiangnan University, 1800 Lihu Road, Wuxi, Jiangsu, 214122, China
[d] Engineering Research Center of Ministry of Education on Food Synthetic Biotechnology, Jiangnan University, 1800 Lihu Road, Wuxi, Jiangsu, 214122, China
[e] Key Laboratory of Carbohydrate Chemistry and Biotechnology, Ministry of Education, Jiangnan University, 1800 Lihu Road, Wuxi, Jiangsu, 214122, China

ARTICLE INFO

Keywords:
OleP
Deoxycholic acid
Hydroxylation
Redox partners
Whole-cell catalysis

ABSTRACT

Deoxycholic acid (DCA) has been authorized by the Federal Drug Agency for cosmetic reduction of redundant submental fat. The hydroxylated product (6β-OH DCA) was developed to improve the solubility and pharmaceutic properties of DCA for further applications. Herein, a combinatorial catalytic strategy was applied to construct a powerful Cytochrome P450 biocatalyst (CYP107D1, OleP) to convert DCA to 6β-OH DCA. Firstly, the weak expression of OleP was significantly improved using pRSFDuet-1 plasmid in the *E. coli* C41 (DE3) strain. Next, the supply of heme was enhanced by the moderate overexpression of crucial genes in the heme biosynthetic pathway. In addition, a new biosensor was developed to select the appropriate redox partner. Furthermore, a cost-effective whole-cell catalytic system was constructed, resulting in the highest reported conversion rate of 6β-OH DCA (from 4.8% to 99.1%). The combinatorial catalytic strategies applied in this study provide an efficient method to synthesize high-value-added hydroxylated compounds by P450s.

1. Introduction

Bile acids and their derivatives (BAs) are a class of steroids, which participate in the digestion and absorption of cholesterol [1]. DCA is an abundant secondary bile acid in the gut with a structure of hydrophobic rigid steroid nuclei [2]. Due to its special chemical structure and biological functions, DCA has a wide range of applications, including cosmetic injection and the prevention of gallstones [3].

However, the water solubility of DCA is poor and a high concentration of DCA can cause oesophageal cancer [4]. Thus, the hydroxylation of DCA is a feasible way to improve its hydrophilicity and eliminate the toxic effect on liver cells [5]. Among various hydroxylated derivatives, the toxicity of 6β-selective hydroxylation of DCA (6β-OH DCA) is lowest and can inhibit the formation of cholesterol gallstones [6]. Currently, although 6β-OH DCA can be obtained from DCA by 11-step chemical synthesis, this method includes repetitious protection and deprotection steps to control the stereoselectivity of hydroxylation, resulting in the inefficient synthetic efficiency (yield lower than 20%) and an environmental threat from many harmful reagents (bromine, chromium trioxide, and methanol, etc.).

Enzymatic catalysis is an alternative strategy to synthesize hydroxylated Bas [7]. Cytochrome P450 enzymes (P450s) are a superfamily of heme-containing metalloenzymes and are capable of stereoselectively catalyzing oxidative reactions of C–H bonds [8]. OleP is a P450 enzyme responsible for the epoxidation of 6-deoxyerythronolide B in the biosynthetic pathway of oleandomycin in *Streptomyces antibioticus* [9]. However, up to now, the highest reported conversion rate of 6β-OH DCA from DCA only could reach 35% using the whole-cell OleP catalytic system [10].

There are several limitations in the application of OleP for the large-scale synthesis of 6β-OH DCA from DCA. The first one is that P450s are easy to misfold to form inactive inclusion bodies [11]. The efficient expression and active folding of OleP requires an appropriate transcriptional rate in microbial cells [12]. In addition, the insufficient

Peer review under responsibility of KeAi Communications Co., Ltd.
* Corresponding author. Science Center for Future Foods, Jiangnan University, 1800 Lihu Road, Wuxi, Jiangsu, 214122, China.
** Corresponding author. Science Center for Future Foods, Jiangnan University, 1800 Lihu Road, Wuxi, Jiangsu 214122, China.
E-mail addresses: gcdu@jiangnan.edu.cn (G. Du), zhaoxinrui@jiangnan.edu.cn (X. Zhao).

https://doi.org/10.1016/j.synbio.2023.11.008
Received 15 October 2023; Received in revised form 12 November 2023; Accepted 18 November 2023
Available online 25 November 2023

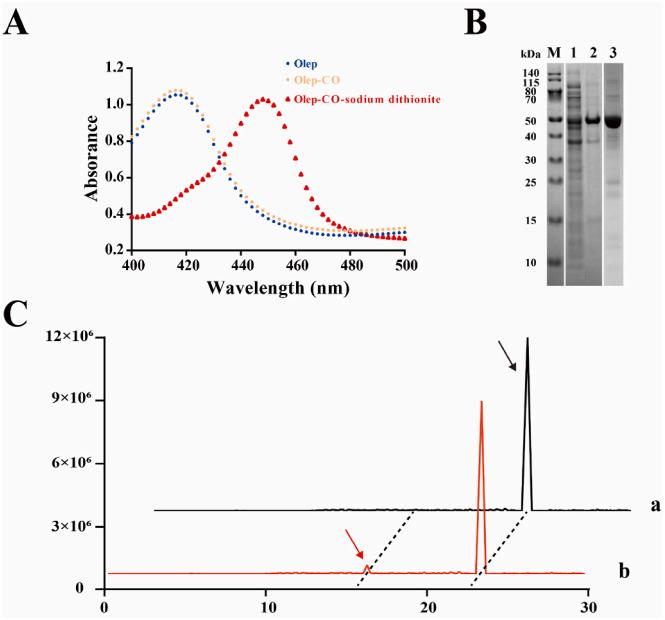

Fig. 1. The characteristics of expressed OleP in *E. coli*. (A) Full wavelength scan of purified OleP in three states. The blue, orange, and red circles mark the characteristic absorbance of the purified OleP, OleP-CO complex, and OleP–CO–sodium dithionite complex, respectively. **(B)** SDS-PAGE analysis of OleP. Lane 1, soluble expression of OleP; Lane 2, inclusion body of OleP; Lane 3, purified soluble OleP. M, marker **(C)** The analysis of the hydroxylated product of DCA catalyzed by OleP. **a** control reaction catalyzed by *E. coli* C43 (DE3) strain harboring pET28a empty plasmid; **b** the hydroxylation of DCA catalyzed by *E. coli* O1 strain harboring pET28a-oleP and pACYC-camA-camB plasmids. The black and red arrows point to the substrate (DCA) and the hydroxylated product (6β-OH DCA), respectively.

supply of heme is another limitation for the preparation of highly active P450s [13]. Heme is the prosthetic group of P450s and is necessary for the catalytic process [14]. However, the concentration of heme is low in the majority of microbial hosts due to the insufficient biosynthesis of heme, limiting the whole-cell OleP biocatalytic activity.

Moreover, the selection of suitable redox partner is crucial for the catalytic reactions mediated by P450s [15]. The redox partner, commonly including ferredoxin (Fdx) and FAD-containing ferredoxin reductase (Fdr), sequentially transfer two electrons from NAD(P)H to the heme-iron reactive center of P450s [16]. However, the optimal redox partner for a specific P450 enzyme is difficult to identify due to the deficiency of an efficient screening method [17]. Thus, it is necessary to develop a new strategy to screen the proper redox partner for P450s whole-cell catalysis.

In this study, 6β-OH DCA was efficiently synthesized from DCA by a robust OleP whole-cell catalyst. In the engineered *E. coli*, the soluble expression level of OleP and the supply of heme were significantly improved. In addition, a split fluorescent sensor was developed to evaluate the suitability between OleP and redox partners. Finally, using the ideal PetH/PetF redox partner, the highest conversion rate (99.1%) of 6β-OH DCA from DCA was achieved in the optimized whole-cell catalytic system of OleP.

2. Results and discussion

2.1. The suitable strategy to express enough OleP for the hydroxylation of DCA in E. coli

Although OleP was successfully expressed in *E. coli* and used as a whole-cell catalyst to synthesize 6β-OH DCA from DCA, the conversion rate was low and the real expressional level of OleP has never been examined [10]. Thus, the proportion of soluble OleP was first detected in this study. In the engineered *E. coli* O1 strain that constructed based on the previously reported method (C43 (DE3) host harboring pET28a-oleP and pACYC-camA-camB plasmids), the expressed OleP presented a characteristic peak at 450 nm after the reaction with sodium dithionite

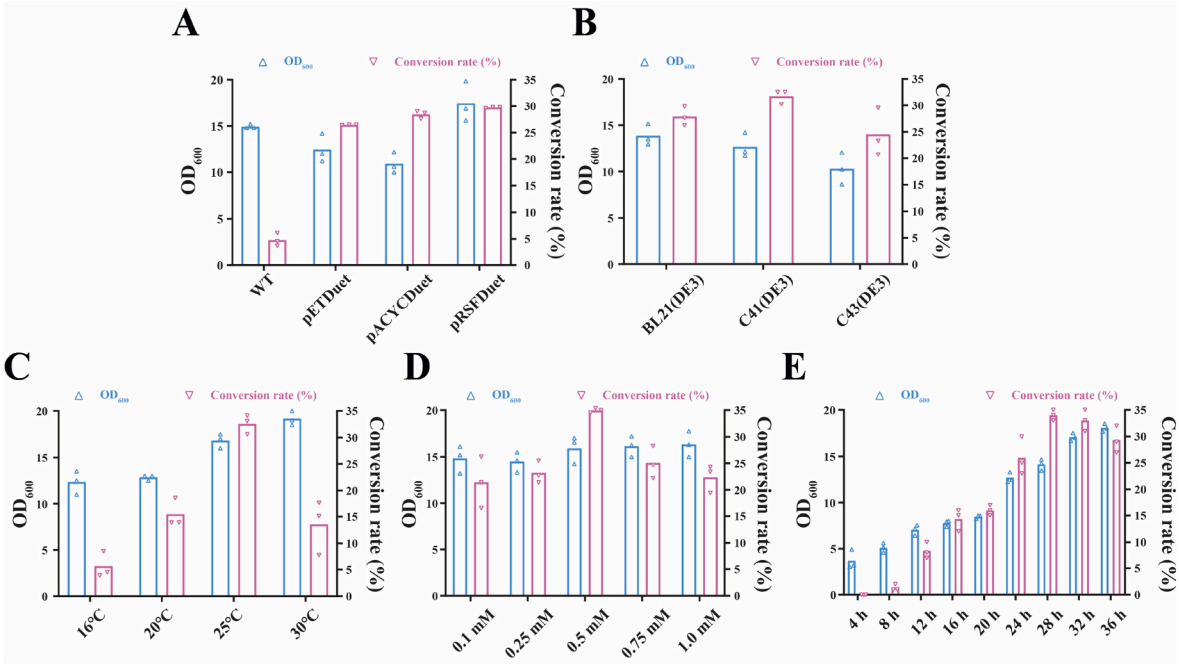

Fig. 2. Three strategies to improve the heterologous expression of OleP in *E. coli*. (A) Selection of suitable plasmid. WT represents the *E. coli* O1 strain. **(B)** Selection of proper host. **(C)** The optimal induction temperature for OleP expression (°C). **(D)** The proper concentration of IPTG for OleP expression (mM). **(E)** The optimal induction time for OleP expression (h). The blue-filled triangle represents the biomass (OD_{600}). The red hollow triangle represents the conversion rate (%). Values and triangles represent the means and standard deviations of biological triplicates.

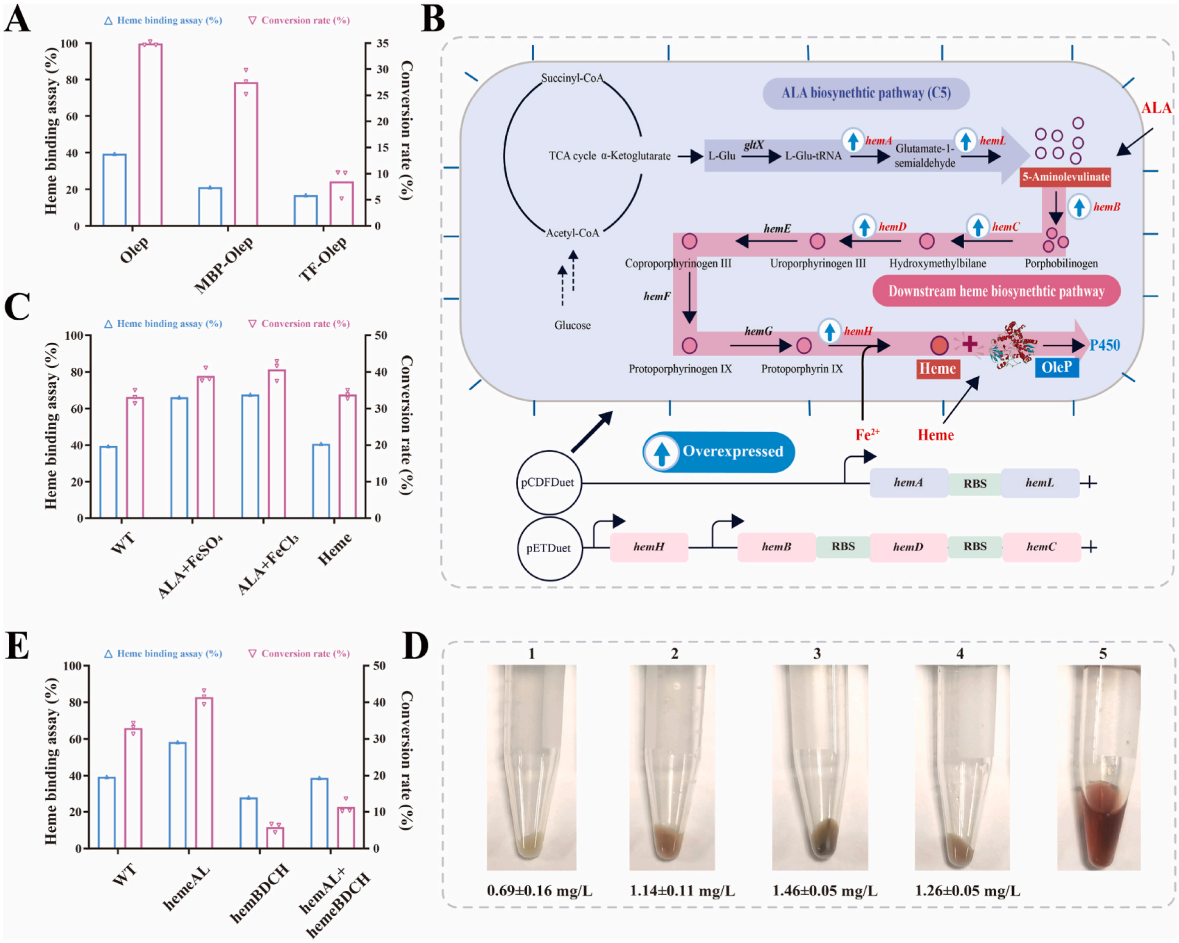

Fig. 3. Strategies to improve heme supply in *E. coli* for the efficient catalysis of OleP. (A) The heme-binding ratio of wild-type OleP, MBP-OleP, and TF-OleP. **(B)** Heme biosynthetic pathways in *E. coli*. The purple arrow represents the C5 pathway and the pink arrow represents the downstream biosynthetic pathway of heme. The pCDFDuet-hemA-hemL plasmid was constructed to enhance the C5 pathway; the pETDuet-hemH-hemB-hemD-hemC plasmid was constructed to enhance the downstream biosynthetic pathway. **(C)** The effect of supplements on the OleP catalysis. **(D)** The color of engineered strains and pure enzyme. **1**: *E. coli* O1 strain; **2**: *E. coli* O2 strain; **3**: *E. coli* O2 strain cultivated with ALA and $FeCl_3$; **4**: *E. coli* AL strain; **5**: OleP enzyme purified from *E. coli* AL strain. The lower values represent the content of intracellular heme in different engineered strains. **(E)** The effect of enhancing heme biosynthesis on the OleP catalysis. The blue-filled triangle represents the heme-binding ratio (%). The red hollow triangle represents the conversion rate (%). Values and triangles represent the means and standard deviations of biological triplicates.

and carbon monoxide (Fig. 1A), but the proportion of soluble OleP only can reach 32.4% (Fig. 1B) [10]. In addition, through the accurate and detailed identification of the hydroxylated product of DCA catalyzed by O1 strain (Figure S1-S7), the whole-cell conversion rate of 6β-OH DCA from DCA is only 4.8% (Fig. 1C). Therefore, it is necessary to improve the active expression of OleP to increase the whole-cell conversion rate.

Four strategies were adopted to enhance the soluble expression of OleP in *E. coli*. Firstly, the selection of proper plasmids and hosts was performed. The results showed that the conversion rate of 6β-OH DCA was significantly increased to 31.7% in the O2 strain (C41 (DE3) host harboring pRSFDuet-camA-camB-oleP plasmid), which was 5.6-fold higher than that obtained in the O1 strain (Fig. 2A and B). Compared with BL21 (DE3) and C43 (DE3) strain, C41 (DE3) strain is beneficial to the folding of P450s due to the moderate attenuated activity of T7 RNA polymerase [12]. In addition, through the prediction of SoluProt (https://loschmidt.chemi.muni.cz/soluprot/), the solubility of OleP could be greatly increased by the fusion expression with MBP (from 41.1% to 92.3%) or TF (from 41.1% to 91.5%) tag (Figure S8) [18]. The results of SDS-PAGE proved the assumption and the soluble expression of OleP was significantly improved. However, the catalytic activity of MBP-OleP **(conversion rate 27.5%)** or TF-OleP **(conversion rate 8.5%)** was maintained at a lower level (Figure S8). Thus, the co-expression of molecular chaperones (pGro7, pKJE7, pGKJE8, PTf16, and pTf2) was applied as an alternative approach, but no chaperone could enhance the catalytic efficiency of OleP (Figure S8) [19]. Furthermore, the conditions of OleP expression were optimized. The results suggested that lower temperature (25°C), moderate concentrations of IPTG (0.5 mM), and specific induction time (28 h) are crucial for OleP expression (67.1% solubility). Under the optimal conditions, the conversion rate of 6β-OH DCA reached 34.8% (Fig. 2C, D, and Fig. 2E).

2.2. Enhancing the heme supply in E. coli to increase conversion rate

To explore the reason for the lower catalytic activity of MBP-OleP and TF-OleP, another important factor (the heme-binding ratio) was detected in these two fused enzymes and wild-type OleP. The results showed that the heme-binding ratio of MBP-OleP and TF-OleP only reached 21.1% and 16.8%, which were much lower than the ratio in the wild-type OleP (39.4%) (Fig. 3A). It indicated that the inefficient supply of heme is the key limiting factor to increase the catalytic efficiency of OleP. In previous research, the adequate supply of heme and high heme-binding ratio are critical for the catalysis of P450s from different sources and there are two main strategies to enhance intracellular heme supply for P450s (Fig. 3B) [13]. One strategy is to supplement the essential

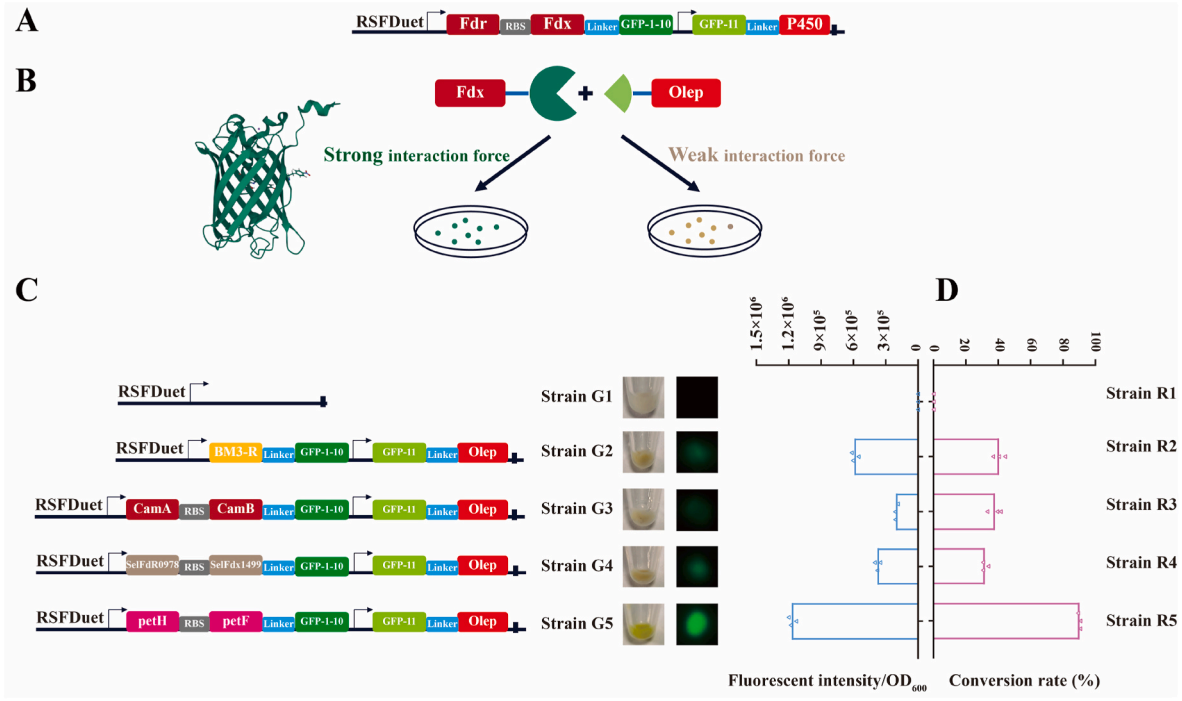

Fig. 4. Strategies to construct sfGFP sensor to screen redox partners. (A) The scheme of constructing the sfGFP sensor. **(B)** The self-assembly of OleP and Fdx was based on the three-dimensional structure of sfGFP (PDB: 5BT0). **(C)** Screening proper redox partners for OleP from different sources. The G1 strain that contains the empty pRSFDuet-1 plasmid was used as a control. The fluorescent intensities were calculated and the color of cells and fluorescent images were presented for G2-G5 strains that express different redox partners-sfGFP-1-10 and sfGFP-11-OleP, respectively. **(D)** The conversion rates were calculated for R2-R5 strains that express different redox partners and OleP, respectively. The R1 strain that contains the empty pRSFDuet-1 plasmid was used as a control. The blue-filled triangle represents the fluorescent intensity/OD_{600}. The red hollow triangle represents the conversion rate (%). Values and triangles represent the means and standard deviations of biological triplicates.

precursor of heme (ALA) during the process of P450s expression and another one is to enhance the heme biosynthetic pathway [20]. In addition, heme can be synthesized through heterologous C4 pathway or endogenous C5 pathway and the C5 pathway has been examined as an efficient way to synthesize heme in *E. coli* [21].

Thus, three combinations of supplements (heme, ALA and $FeSO_4$, ALA and $FeCl_3$) were added to improve intracellular heme supply at first. As *E. coli* lacks the uptake system of heme, the supplement of heme cannot be efficiently utilized and the heme-binding ratio (40.8%) and the conversion rate of 6β-OH DCA (33.8%) nearly maintained at the similar level without heme addition (Fig. 3C) [22]. Moreover, the combination of supplementing ALA and $FeSO_4$ or $FeCl_3$ have the same positive effect on the catalysis of OleP. With the improvement of heme supply in the cells, the colors of engineered strains turned to dark red (Fig. 3D) and the highest heme-binding ratio (67.7%) and the conversion rate of 6β-OH DCA (40.7%) was obtained when ALA and $FeCl_3$ were added (Fig. 3C). However, the addition of ALA accounts for 60% of the cost of whole-cell catalysis [12]. Therefore, the enhancement of heme biosynthesis is a more cost-effective approach to increase heme supply and catalytic efficiency.

Based on the analysis of main rate-limiting enzymes in heme biosynthetic pathway, *hemA* and *hemL* that involves in the synthesis of ALA (C5 pathway) and *hemB*, *hemC*, *hemD*, and *hemH* that involves in the downstream heme biosynthetic pathway should be enhanced to increase the intracellular heme supply [23]. Thus, three related engineered strains were constructed, including *E. coli* AL strain (*E. coli* O2 strain enhancing *hemA* and *hemL*), *E. coli* BCDH strain (*E. coli* O2 strain enhancing *hemB*, *hemC*, *hemD*, and *hemH*) and *E. coli* AL-BCDH strain (*E. coli* O2 strain enhancing all rate-limiting enzymes). Although the color of *E. coli* AL strain turned to light red (Fig. 3D) and the heme-binding ratio slightly reduced to 53.9%, the overexpression of *hemA* and *hemL* could increase the conversion rate of 6β-OH DCA to 41.4%, which is similar with the effect of supplementing ALA and $FeCl_3$ (Fig. 3E). Nevertheless, the overexpression of *hemB*, *hemC*, *hemD*, and *hemH* was not necessary for OleP catalysis because the conversion rate of 6β-OH DCA dramatically decreased in both *E. coli* BCDH (supplementing ALA and $FeCl_3$) and AL-BCDH strains, which might be caused by the excessive metabolic burden to the host. Therefore, the *E. coli* AL strain was selected to perform further optimizations to achieve a higher conversion rate of OleP.

2.3. Screening the optimal redox partner for OleP by bimolecular fluorescence complementation technology (BiFC)

Besides the self-sufficient P450s (BM3, etc.) [24], a majority of typical reactions catalyzed by P450s require a pair of redox partner (FdR and Fdx) that transfer electrons to heme-iron reactive center, which is vital for the catalytic efficiency of P450s [16]. However, the most suitable redox partner for a special P450 is difficult to select because it is hard to assess the degree of adaptation between P450s and redox partner. In previous research, the BiFC technique has been used to detect the change of distance between the P450 enzyme and modified redox partner, but this method is not applicable to evaluate the suitability of redox partners due to the lower sensitivity of fused yellow fluorescent protein (YFP) [17].

BiFC technique relies on the interactions between the bait and prey proteins that combine two non-fluorescent split protein domains and subsequently co-folding into the β-barrel structure to form the chromophore [25]. Thus, a more sensitive and easily detectable sfGFP (a superfolding derivative of GFP) sensor was designed and applied to measure the interaction between OleP and redox partners [26]. The Fdx was fused to the N-terminal of sfGFP-1-10, while OleP was fused to the C-terminal of sfGFP-11 (Fig. 4A). When the interaction between OleP and Fdx is strong, two non-fluorescent split proteins (sfGFP-1-10 and

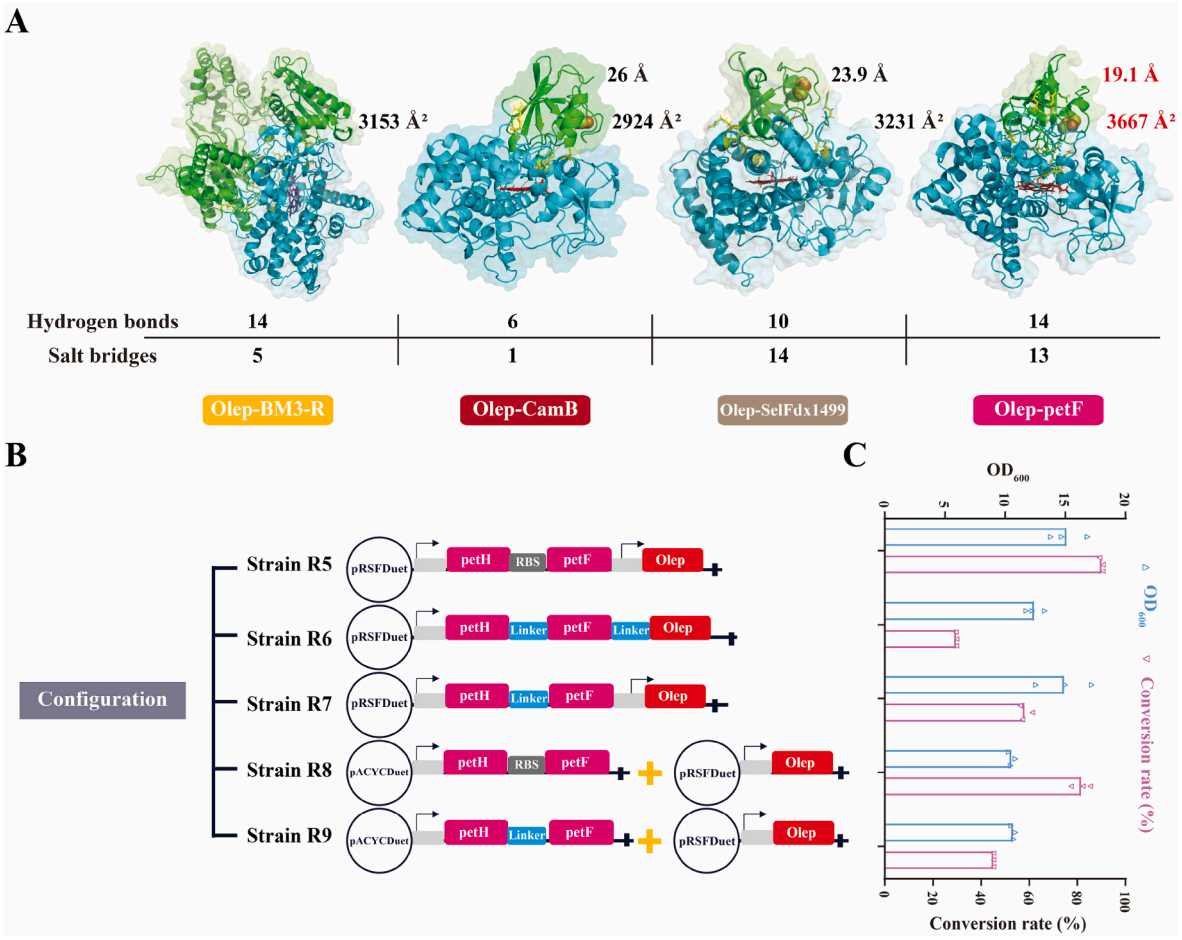

Fig. 5. The simulated analysis and design of redox partners for OleP. (A) The structures and interactions between OleP and Fdxs are presented. The key interacting residues in OleP-Fdx complexes are depicted as sticks and highlighted in yellow. Heme and substrates are displayed as sticks, colored in red and wheat, respectively. The Fe_2S_2 cluster is visualized as spheres. The distances (Å) between the iron-sulfur cluster and heme-iron are measured and indicated by dashed red lines. The interaction areas of OleP-Fdx are calculated by NovoPro (https://www.novopro.cn/). The numbers of hydrogen bonds and salt bridges are predicted by PDBePISA (https://www.ebi.ac.uk/pdbe/). **(B)** The fusion expression and the different expressional ratios between OleP and PetH/PetF. **(C)** The conversion rate of DCA for R5-R9 strains. The blue-filled triangle represents the biomass (OD_{600}). The red hollow triangle represents the conversion rate (%). Values and triangles represent the means and standard deviations of biological triplicates.

sfGFP-11) will form the chromophore and green fluorescence could be detected (Fig. 4B). In this study, four different redox partners were tested for OleP, including the reductase domain of BM3 (G2 strain) [27], the most commonly used CamA/CamB (G3 strain) and SelF-dx1499/SelFdR0978 (G4 strain) in *E. coli* [28], high-active PetH/PetF from *Synechocystis* sp. PCC6803 (G5 strain) (Fig. 4C) [29].

Based on the new sfGFP sensor, PetH/PetF was selected as the most proper redox partner for OleP. Compared with the control (G1 strain), the value of fluorescence intensity/OD_{600} between OleP and PetH/PetF reached 1.2×10^6, which is 6-fold higher than the value between OleP and original CamA/CamB (Fig. 4D). The green fluorescence of the G5 strain can be seen either by fluorescence microscope or by eyes (Fig. 4C). In addition, five additional engineered strains that fused sfGFP were removed from the complexes of OleP and Fdxs (R1-R5 strains) were constructed to detect the effect of different Fdxs on the hydroxylation of DCA. Applying PetH/PetF as a redox partner (R5 strain), the conversion rate of DCA significantly increased to 89.2% by whole-cell catalysis, further proving the availability of a newly constructed sfGFP sensor (Fig. 4D). The results indicated that the novel sfGFP sensor can be applied as a rapid and simple method to screen and redesign redox partners to enhance the catalytic efficiency of P450s.

To elucidate the advantage of PetH/PetF in the catalysis of OleP, the interactions between OleP and different Fdxs were analyzed by simulating the OleP-Fdx complexes using the GRAMM Server [30]. In previous studies, it has been proven that the interaction between P450 and ferredoxin is influenced by the electrostatic forces and the distance between iron-sulfur cluster and heme-iron [28]. Based on the simulated results, the OleP-petF complex exhibited a larger interface area of 3667.2 $Å^2$ and significantly stronger hydrogen bonds (14) and salt bridges (13), leading to a much shorter distance between Fe_2S_2 and heme-iron (19.1 Å) than the other three complexes (Fig. 5A).

As the interaction distance between OleP and the redox partner is crucial for its catalytic efficiency, a flexible linker $(GGGGS)_2$ was used to bind OleP with PetF together. In addition, the expressional ratio between OleP and PetH/PetF was also optimized to obtain the best catalytic effect (R6-R9 strains, Fig. 5B). However, the results showed that the linkage of OleP and PetH/PetF led to an obvious reduction in the conversion rate of DCA, suggesting that the fusion expression reduced the activity of OleP (Fig. 5C). As for the expressional ratio between OleP and PetH/PetF, it indicated that it is necessary to maintain a high expressional level of PetH/PetF using the high-copy number pRSFDuet-1 plasmid to match the requirement of catalysis for OleP (Fig. 5C). This result was consistent with the previous conclusions for the other P450s (CYP109B1 [31] and P450sca-2 [27], etc.) and thus R5 strain was selected to perform the following optimization.

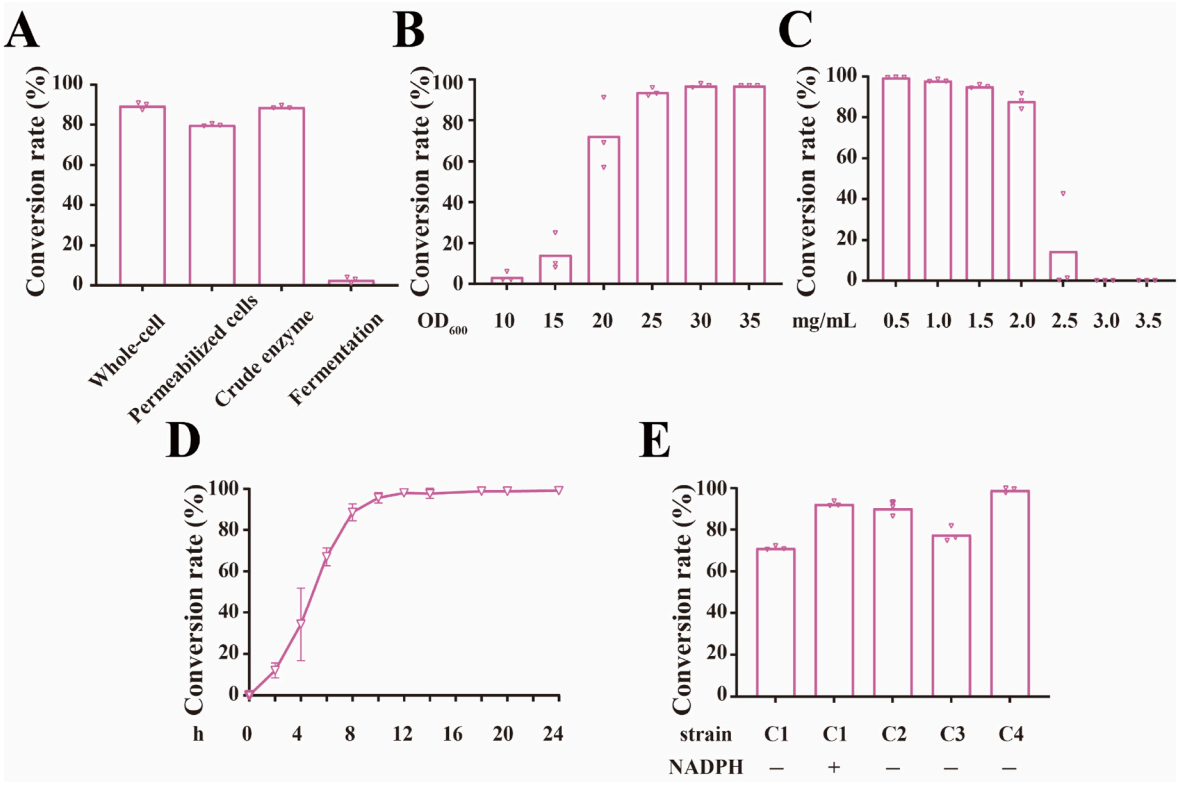

Fig. 6. The optimal whole-cell catalytic system for OleP catalysis. (A) Effect of catalytic form. **(B)** Effect of different biomass of resting whole-cell (OD_{600}). **(C)** Effect of concentration of DCA (mg/mL). **(D)** Effect of catalytic time (h). **(E)** Effect of NADPH addition and intracellular NADPH regeneration system. The red hollow triangle represents the conversion rate (%). Values and triangles represent the means and standard deviations of biological triplicates.

2.4. The optimal whole-cell catalytic system for OleP to perform the most efficient conversion

Based on the strategies used in AL and R5 strains, a highly active *E. coli* C1 strain that harbors pRSFDuet-petH-petF-oleP and pCDFDuet-hemA-hemL plasmids was obtained and the conversion rate could reach 89.7% without supplementing ALA and $FeCl_3$. To further improve the catalytic efficiency of OleP, the whole-cell catalytic system was optimized, including the catalytic form, the biomass of C1 strain whole-cell, the concentration of substrate (DCA), the catalytic time, and the

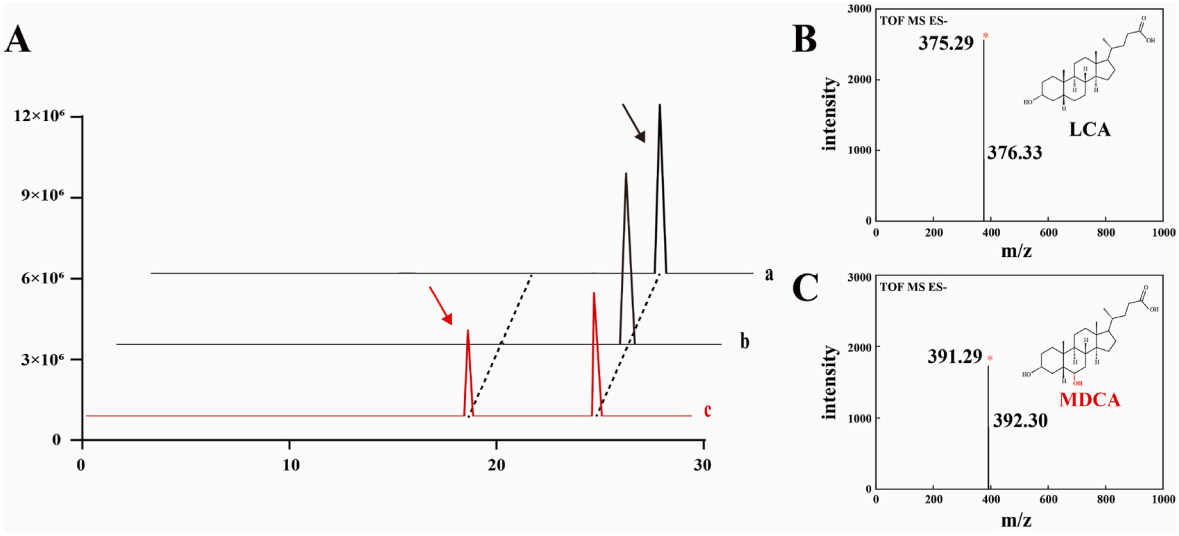

Fig. 7. LCMS analysis of the hydroxylation of LCA by OleP. (A) Biocatalytic reaction of LCA. **a** control reaction catalyzed by *E. coli* C41 (DE3) strain harboring pRSFDuet-1 empty plasmid; **b** the hydroxylation of LCA catalyzed by *E. coli* O1 strain harboring pET28a-oleP and pACYCDuet-camA-camB plasmids; **c** the hydroxylation of LCA catalyzed by *E. coli* C4 strain harboring pRSFDuet-petH-petF-oleP, pCDFDuet-hemA-hemL, and pACYCDuet-pntAB-nadK plasmids. The black and red arrows point to the substrate (LCA) and the hydroxylated product (MDCA), respectively. **(B)** MS analysis of substrate LCA. **(C)** MS analysis of hydroxylated product MDCA.

supply of NADPH cofactor [32]. The results showed that 2.0 mg/mL DCA could be catalyzed by C1 strain whole-cell (biomass $OD_{600} = 30$) to 1.85 mg/mL 6β-OH DCA (92.5% conversion rate) in 12 h (Fig. 6A–D).

In addition, it found that the conversion rate dramatically decreased to 71.2% without NADPH addition (Fig. 6E), indicating the requirement of intracellular NADPH supply for OleP catalysis. Furthermore, to further reduce the cost of NADPH addition, the expression of NAD^+ kinase (NadK) or membrane-bound transhydrogenase (PntAB) was attempted to enhance intracellular NADPH regeneration [33,34]. The results showed that the conversion rates were increased from 71.2% (C1 strain without NADPH addition) to 90.3% in C2 strain (C1 strain harboring pACYCDuet-nadK plasmid) and to 77.6% in C3 strain (C1 strain harboring pACYCDuet-pntAB plasmid), respectively. Thus, NadK and PntAB were co-expressed in the C4 strain (C1 strain harboring pACYCDuet-pntAB-nadK plasmid) and the final conversion rate of DCA to 6β-OH DCA reached 99.1% without NADPH addition, which is more efficient than the best reported result so far (conversion rate of 35%) [10].

To further verify whether the obtained whole-cell catalytic system for OleP can be applicable to catalyze the hydroxylation of other bile acids, LCA was further hydroxylated to produce murideoxycholic acid (MDCA), which can inhibit the accumulation of cholesterol in serum and liver (Table S3) [6]. Through the detection of LCMS, the conversion rate of LCA prepared by O1 strain was only 1.6% (Fig. 7A–C). The conversion rate of LCA to MDCA significantly increased to 42.7% by using the optimal whole-cell catalytic system for C4 strain (Fig. 7A). Therefore, the constructed efficient catalytic system for OleP is a promising biocatalyst for the synthesis of 6β-hydroxylated products of BAs.

3. Conclusion

In summary, an efficient whole-cell P450 biocatalyst was obtained by improving the soluble expressional level of OleP, enhancing the intracellular heme supply, establishing a new biosensor to screen a suitable pair of redox partner for OleP, and optimizing the whole-cell catalytic conditions. The final engineered *E. coli* C4 strain that harbors pRSFDuet-petH-petF-oleP, pCDFDuet-hemA-hemL, and pACYCDuet-pntAB-nadK plasmids has a strong ability of hydroxylation, achieving the conversion rate of 99.1% for 6β-OH DCA and 42.7% for MDCA using DCA and LCA as substrates, respectively. The combinatorial catalytic strategies used in this study offer insights into enhancing the catalytic efficiency of other P450s.

CRediT authorship contribution statement

Chixiang Sun: Investigation, Data curation, Writing – original draft. **Baodong Hu:** Investigation, Data curation. **Yanchun Li:** Data curation. **Zhimeng Wu:** Supervision. **Jingwen Zhou:** Supervision. **Jianghua Li:** Supervision. **Jian Chen:** Supervision. **Guocheng Du:** Supervision, Validation. **Xinrui Zhao:** Funding acquisition, Supervision, Validation.

Declaration of competing interest

The authors declare that they have no known competing financial interests or personal relationships that could have appeared to influence the work reported in this paper.

Acknowledgments

This work was supported by the National Key Research and Development Program of China (2019YFA0906400) and the National First-class Discipline Program of Light Industry Technology and Engineering (LITE2018-08), Postgraduate Research & Practice Innovation Program of Jiangsu Province (KYCX23_2486). We thank Prof. Shengying Li (Shandong University, China) for providing plasmids pET28a-SelFdx1499 and pET28a-SelFdR0978.

Appendix A. Supplementary data

Supplementary data to this article can be found online at https://doi.org/10.1016/j.synbio.2023.11.008.

References

[1] Hofmann AF, Hagey LR, Krasowski MD. Bile salts of vertebrates: structural variation and possible evolutionary significance. J Lipid Res 2010;51(2):226–46. https://doi.org/10.1194/jlr.R000042.
[2] Ajouz H, Mukherji D, Shamseddine A. Secondary bile acids: an underrecognized cause of colon cancer. World J Surg Oncol 2014;12:1–5. https://doi.org/10.1186/1477-7819-12-164. Artn 164.
[3] Sykes JM, Allak A, Klink B. Future applications of deoxycholic acid in body contouring. J Drugs Dermatol 2017;16(1):43–6. https://doi.org/10.1007/s40257-016-0231-3.
[4] Hofmann AF, Herdt T, Ames NK, Chen Z, Hagey LR. Bile acids and the microbiome in the cow: lack of deoxycholic acid hydroxylation. Lipids 2018;53(3):269–70. https://doi.org/10.1002/lipd.12036.
[5] Wietholtz H, Marschall HU, Sjovall J, Matern S. Stimulation of bile acid 6 alpha-hydroxylation by rifampin. J Hepatol 1996;24(6):713–8. https://doi.org/10.1016/S0168-8278(96)80268-6.
[6] Cohen BI, Matoba N, Mosbach EH, Ayyad N, Hakam K, Suh SO, McSherry CK. Bile acids substituted in the 6 position prevent cholesterol gallstone formation in the hamster. Gastroenterology 1990;98(2):397–405. https://doi.org/10.1016/0016-5085(90)90831-k.
[7] Acevedo-Rocha CG, Gamble CG, Lonsdale R, Li A, Nett N, Hoebenreich S, Lingnau JB, Wirtz C, Fares C, Hinrichs H, et al. P450-catalyzed regio- and diastereoselective steroid hydroxylation: efficient directed evolution enabled by mutability landscaping. ACS Catal 2018;8(4):3395–410. https://doi.org/10.1021/acscatal.8b00389.
[8] Hu B, Zhao X, Wang E, Zhou J, Li J, Chen J, Du G. Efficient heterologous expression of cytochrome P450 enzymes in microorganisms for the biosynthesis of natural products. Crit Rev Biotechnol 2023;43(2):227–41. https://doi.org/10.1080/07388551.2022.2029344.
[9] Gaisser S, Lill R, Staunton J, Mendez C, Salas J, Leadlay PF. Parallel pathways for oxidation of 14-membered polyketide macrolactones in *Saccharopolyspora erythraea*. Mol Microbiol 2002;44(3):771–81. https://doi.org/10.1046/j.1365-2958.2002.02910.x.
[10] Grobe S, Wszolek A, Brundiek H, Fekete M, Bornscheuer UT. Highly selective bile acid hydroxylation by the multifunctional bacterial P450 monooxygenase CYP107D1 (OleP). Biotechnol Lett 2020;42(5):819–24. https://doi.org/10.1007/s10529-020-02813-4.
[11] Zelasko S, Palaria A, Das A. Optimizations to achieve high-level expression of cytochrome P450 proteins using *Escherichia coli* expression systems. Protein Expr Purif 2013;92(1):77–87. https://doi.org/10.1016/j.pep.2013.07.017.
[12] Angius F, Ilioaia O, Amrani A, Suisse A, Rosset L, Legrand A, Abou-Hamdan A, Uzan M, Zito F, Miroux B. A novel regulation mechanism of the T7 RNA polymerase based expression system improves overproduction and folding of membrane proteins. Sci Rep 2018;8(1):8572. https://doi.org/10.1038/s41598-018-26668-y.
[13] Zhao XR, Choi KR, Lee SY. Metabolic engineering of *Escherichia coli* for secretory production of free haem. Nat Catal 2018;1(9):720–8. https://doi.org/10.1038/s41929-018-0126-1.
[14] Honda Y, Nanasawa K, Fujii H. Coexpression of 5-aminolevulinic acid synthase gene facilitates heterologous production of thermostable cytochrome P450, CYP119, in holo form in *Escherichia coli*. Chembiochem 2018;19(20):2156–9. https://doi.org/10.1002/cbic.201800331.
[15] Reisky L, Buchsenschutz HC, Engel J, Song T, Schweder T, Hehemann JH, Bornscheuer UT. Oxidative demethylation of algal carbohydrates by cytochrome P450 monooxygenases. Nat Chem Biol 2018;14(4):342–4. https://doi.org/10.1038/s41589-018-0005-8.
[16] Li S, Du L, Bernhardt R. Redox partners: function modulators of bacterial P450 enzymes. Trends Microbiol 2020;28(6):445–54. https://doi.org/10.1016/j.tim.2020.02.012.
[17] Xu Y, Wang X, Zhang C, Zhou X, Xu X, Han L, Lv X, Liu Y, Liu S, Li J, et al. De novo biosynthesis of rubusoside and rebaudiosides in engineered yeasts. Nat Commun 2022;13(1):3040. https://doi.org/10.1038/s41467-022-30826-2.
[18] Hon J, Marusiak M, Martinek T, Kunka A, Zendulka J, Bednar D, Damborsky J. SoluProt: prediction of soluble protein expression in *Escherichia coli*. Bioinformatics 2021;37(1):23–8. https://doi.org/10.1093/bioinformatics/btaa1102.
[19] Hartl FU, Hayer-Hartl M. Molecular chaperones in the cytosol: from nascent chain to folded protein. Science 2002;295(5561):1852–8. https://doi.org/10.1126/science.1068408.
[20] Michener JK, Nielsen J, Smolke CD. Identification and treatment of heme depletion attributed to overexpression of a lineage of evolved P450 monooxygenases. Proc Natl Acad Sci U S A 2012;109(47):19504–9. https://doi.org/10.1073/pnas.1212287109.
[21] Lindman S, Hernandez-Garcia A, Szczepankiewicz O, Frohm B, Linse S. In vivo protein stabilization based on fragment complementation and a split GFP system. Proc Natl Acad Sci U S A 2010;107(46):19826–31. https://doi.org/10.1073/pnas.1005689107.
[22] Fiege K, Querebillo CJ, Hildebrandt P, Frankenberg-Dinkel N. Improved method for the incorporation of heme cofactors into recombinant proteins using *Escherichia*

coli Nissle 1917. Biochemistry 2018;57(19):2747–55. https://doi.org/10.1021/acs.biochem.8b00242.
[23] Choi KR, Yu HE, Lee H, Lee SY. Improved production of heme using metabolically engineered *Escherichia coli*. Biotechnol Bioeng 2022;119(11):3178–93. https://doi.org/10.1002/bit.28194.
[24] Whitehouse CJ, Bell SG, Wong LL. P450(BM3) (CYP102A1): connecting the dots. Chem Soc Rev 2012;41(3):1218–60. https://doi.org/10.1039/c1cs15192d.
[25] Pang C, Zhang G, Liu S, Zhou J, Li J, Du G. Engineering sigma factors and chaperones for enhanced heterologous lipoxygenase production in *Escherichia coli*. Biotechnol Biofuels Bioprod 2022;15(1):105. https://doi.org/10.1186/s13068-022-02206-x.
[26] Mo HM, Xu Y, Yu XW. Improved soluble expression and catalytic activity of a thermostable esterase using a high-throughput screening system based on a split-GFP assembly. J Agric Food Chem 2018;66(48):12756–64. https://doi.org/10.1021/acs.jafc.8b04646.
[27] Hu B, Zhao X, Zhou J, Li J, Chen J, Du G. Efficient hydroxylation of flavonoids by using whole-cell P450 sca-2 biocatalyst in *Escherichia coli*. Front Bioeng Biotech 2023;11:1138376. https://doi.org/10.3389/fbioe.2023.1138376.
[28] Liu X, Li F, Sun T, Guo J, Zhang X, Zheng X, Du L, Zhang W, Ma L, Li S. Three pairs of surrogate redox partners comparison for Class I cytochrome P450 enzyme activity reconstitution. Commun Biol 2022;5(1):791. https://doi.org/10.1038/s42003-022-03764-4.
[29] Kern F, Dier TK, Khatri Y, Ewen KM, Jacquot JP, Volmer DA, Bernhardt R. Highly efficient CYP167A1 (EpoK) dependent epothilone B formation and production of 7-ketone epothilone D as a new epothilone derivative. Sci Rep 2015;5:14881. https://doi.org/10.1038/srep14881.
[30] Katchalskikatzir E, Shariv I, Eisenstein M, Friesem AA, Aflalo C, Vakser IA. Molecular-surface recognition-determination of geometric fit between proteins and their ligands by correlation techniques. Proc Natl Acad Sci U S A 1992;89(6):2195–9. https://doi.org/10.1073/pnas.89.6.2195.
[31] Zhang XD, Hu Y, Peng W, Gao CH, Xing Q, Wang BJ, Li AT. Exploring the potential of cytochrome P450 CYP109B1 catalyzed regio-and stereoselective steroid hydroxylation. Front Chem 2021;9:649000. https://doi.org/10.3389/fchem.2021.649000. ARTN 649000.
[32] You ZN, Chen Q, Shi SC, Zheng MM, Pan J, Qian XL, Li CX, Xu JH. Switching cofactor dependence of 7β-hydroxysteroid dehydrogenase for cost-effective production of ursodeoxycholic acid. ACS Catal 2018;9(1):466–73. https://doi.org/10.1021/acscatal.8b03561.
[33] Deng H, Gao S, Zhang W, Zhang T, Li N, Zhou J. High titer of (S)-equol synthesis from daidzein in *Escherichia coli*. ACS Synth Biol 2022;11(12):4043–53. https://doi.org/10.1021/acssynbio.2c00378.
[34] Li W, Wu H, Li M, San KY. Effect of NADPH availability on free fatty acid production in *Escherichia coli*. Biotechnol Bioeng 2018;115(2):444–52. https://doi.org/10.1002/bit.26464.